JOURNAL OF MATERIALS SCIENCE 8 (1973) 1030–1040

Prediction of ion-bombarded surface topographies using Frank's kinematic theory of crystal dissolution

D. J. BARBER, F. C. FRANK*, M. MOSS*, J. W. STEEDS*, I. S. T. TSONG
Department of Physics, University of Essex, Colchester, UK
**H. H. Wills Physics Laboratory, University of Bristol, Bristol, UK*

The two kinematic theorems of crystal dissolution by Frank are applied to surfaces undergoing ion-bombardment in order to determine the topographies evolved in any given time. The predicted shapes show good agreement with experimental observations.

1. Introduction

In recent years there has been a growing interest in the study of ion bombardment of solid surfaces largely because of practical applications, which include the ion thinning of specimens for transmission electron microscopy [1, 2] and the ion polishing and shaping of optical surfaces [3, 4]. Numerous experiments have been carried out to investigate the development of surface topographies on ion-bombarded amorphous and crystalline targets [5-12]. A treatment of the problem by computer simulation has also been reported [13]. The appearance of topographic features such as cones, pits, hillocks and hummocks is generally explained by variations of the sputtering rate across the surface due to initial surface irregularities or small foreign particles resting on the target surface. The usual assumption made is that surface erosion is caused by sputtering only, i.e. other processes such as surface diffusion, local variation of binding energy over a surface, and redeposition of sputtered material are ignored. In this paper a treatment of this problem making these assumptions is presented which shows that ion-bombarded surface topographies can be predicted easily using Frank's kinematic theory of the orientation-dependent dissolution of crystals [14, 15].

2. Theory

Frank's two theorems on crystal dissolution will be well known to those who have studied chemical etching. We shall restate them here for the benefit of workers in sputtering who might not be familiar with them. The first of the dissolution theorems states that if the rate of dissolution of a crystal surface at any given time is a function only of orientation, then during dissolution, the locus of an elemental area of crystal surface with a particular orientation is a straight line. We call any such locus a dissolution trajectory. The second theorem states that if the dissolution rate is defined as measured normal to the actual crystal surface, and the polar diagram of the reciprocal of this dissolution rate as a function of orientation is constructed, then the trajectory of an elemental area of crystal surface of given orientation is parallel to the normal to the polar diagram at the point of corresponding orientation. One corollary arising out of these two theorems is that when there is a discrete change of orientation between adjacent elements of area, such a crystal edge, its dissolution trajectory is given by the normal to a chord of the polar diagram joining the points corresponding to the orientations of these two adjacent elements. The mathematical proofs of these theorems in both two and three dimensions are to be found in Frank's original papers [14, 15].

One immediately sees that the similarity between sputtering and chemical etching lies in the fact that the erosion rate of a given element of specimen surface due to sputtering also depends on the orientation of that element, which is usually expressed as the variation of sputtering yield with the angle of incidence of the ion beam.

3. Application to glasses: isotropic case

Frank's theorems have been successfully applied to interpret experimental results on the dissolution of crystals [16, 17]. We shall proceed to demonstrate that they are equally applicable to the erosion of surfaces by ion bombardment, starting with the case of glasses.

If θ is the angle which the ion beam makes with the normal to the target surface, then the sputtering yield, S, defined as the number of sputtered atoms per incoming ion, can be expressed as a function of θ. The depth, d, sputtered from a plane surface is given by

$$d = \frac{\Phi t}{n} S(\theta) \cos \theta \qquad (1)$$

where Φ is the number of ions per second striking unit area of surface normal to their direction, n is the number of atoms per unit volume of target material, and t is the time of bombardment. Since we are interested in the thickness of material removed by sputtering rather than the number of atoms ejected from the surface at any given time, it is convenient to plot $S(\theta)\cos\theta/S(0)$ against θ. Fig. 1 shows such a plot for the case of a silica glass surface bombarded by Ar^+ ions (data taken from Bach [18]). We choose silica glass as the subject of our study since it is single-phase and non-crystalline and we can make the assumption that the amount of surface eroded is entirely dependent on the inclination of the ion beam to the surface. We shall apply Frank's theorem to two general situations in ion bombardment; (1) the incident ion beam is perpendicular to the target surface, i.e. $\theta = 0$, corresponding to the case in which the majority of experimental studies on sputtering phenomenon were carried out; (2) the ion beam is at $\theta = 60°$ to the target surface which is rotated in its plane about an axis through its centre. This corresponds to the case in ion thinning.

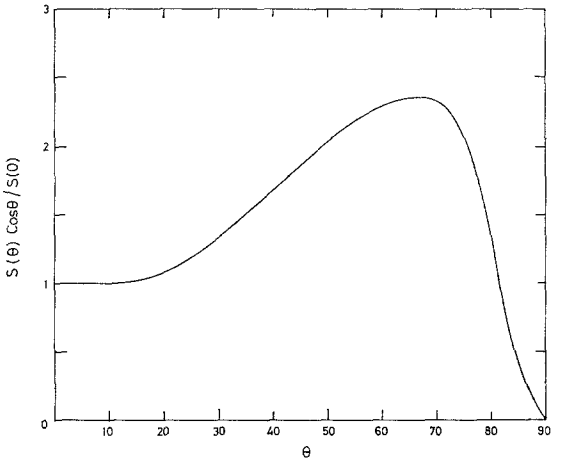

Figure 1 Variation of sputtering ratio with angle of incidence for Ar^+ ions on silica glass, derived from experimental results of Bach [18].

3.1. Normal incidence

From the data in Fig. 1, we can plot the reciprocals of the sputtering ratio $S(\theta)\cos\theta/S(0)$ on polar graph paper in accordance with the second theorem of Frank. This we shall call the "erosion slowness" polar diagram and it is shown in Fig. 2. Given a particular starting surface shape, we are now able to deduce the successive sputtered topographies for silica glass.

First let us consider the case of a glass sphere which is represented in two dimensions by a circle on polar graph paper. The starting circular shape shown in Fig. 2 is conveniently superimposed on the erosion slowness curve. The next step is to draw the orientation trajectories which obey the dissolution theorems. These trajectories are parallel to the direction of the normals to the slowness curve at corresponding orientations. They are drawn inwards towards the inside of the circle because of the erosion caused by ion bombardment. According to Frank [14, 16] the interpretation in terms of the crystal surface, when two trajectories representing different orientations meet in space, must be that a discontinuity, i.e., an edge, is produced. These edge trajectories are not necessarily straight. Hence, in Fig. 2, when two trajectories meet, their lines are erased beyond the meeting point and the direction of the resulting trajectory is drawn normal to the chord joining points of corresponding orientations on the erosion slowness curve.

The final step is to derive resultant topographies at any given time during bombardment from the trajectory array constructed. First we start with the 0° orientation on the initial circular profile of the sphere, i.e., normal incidence, marking off on the trajectory the distance corresponding to the depth eroded appropriate to a given bombardment time. For other orientations we place one edge of a pair of parallel rules at a tangent to the initial profile. This selects a point on the profile corresponding to a particular surface orientation. We then side-step the parallel rules along the trajectory from that orientation for a distance appropriate

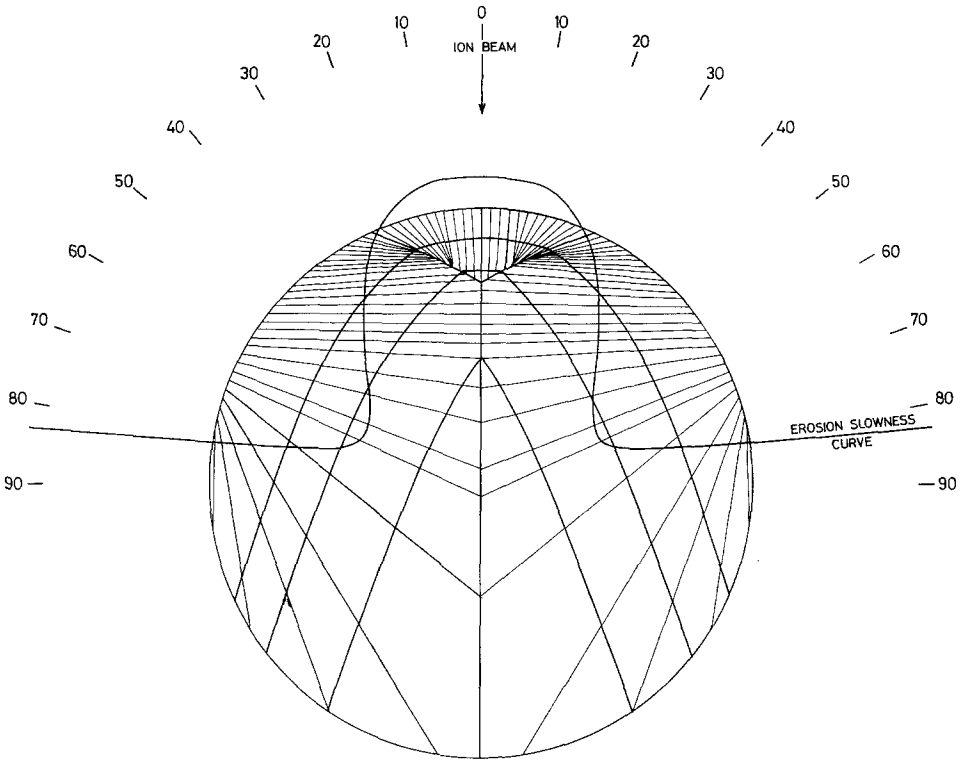

Figure 2 Polar diagram of the reciprocal sputtering ratio for silica (erosion slowness curve) and the "dissolution" trajectories and derived profiles for the sputtering of a silica glass sphere.

to the same bombardment time as that for normal incidence. This distance is some multiple of the distance for 0° orientation as determined from the sputtering curve (Fig. 1). Then according to Franks' first theorem [14] the rule is still at a tangent to the evolving surface and this new position of the surface element can be marked off on the trajectory. An alternative method of constructing the resultant profiles is to start from a point in one trajectory (determined by a chosen bombardment time) by drawing a line parallel to the tangent to the initial profile until this line meets the next trajectory and then repeating the same operation starting from this new point. If the trajectories are sufficiently close together, we can continue the profile in the right direction at every point by successive small steps without ever measuring distance along a trajectory or referring again to the sputtering curve. Of the two methods of construction, the second one is easier to execute. In the present paper, both methods were used in deducing the sputtered profiles, with one serving as a check for the other.

Three resultant shapes of the bombarded surface are shown in Fig. 2; the first corresponds to the shape after a short time of bombardment and the second and third correspond to longer periods. These shapes agree quite well with the experimental observations on ion bombarded metal spheres by Wehner [19]. The isotropic theory is presumably applicable on account of the small grain size of the material. Differences are probably due to the effects of impurities at the cone tips.

Figs. 3 and 4 show similar treatment applied to a hemispherical trough and a sinusoidal surface respectively. Sputtering of a deep trough (Fig. 3a) will turn it into a shaft-like depression with vertical walls and a flat bottom whereas sputtering of a shallower trough (Fig. 3b) will result in the widening of the trough and decrease of the slope. These profiles agree reasonably well with the observations by Bayly [7] even though we have not taken into account the secondary effects such as ion reflection and redeposition. In Fig. 4 the evolution of the sputtered shapes from the initial sinusoidal

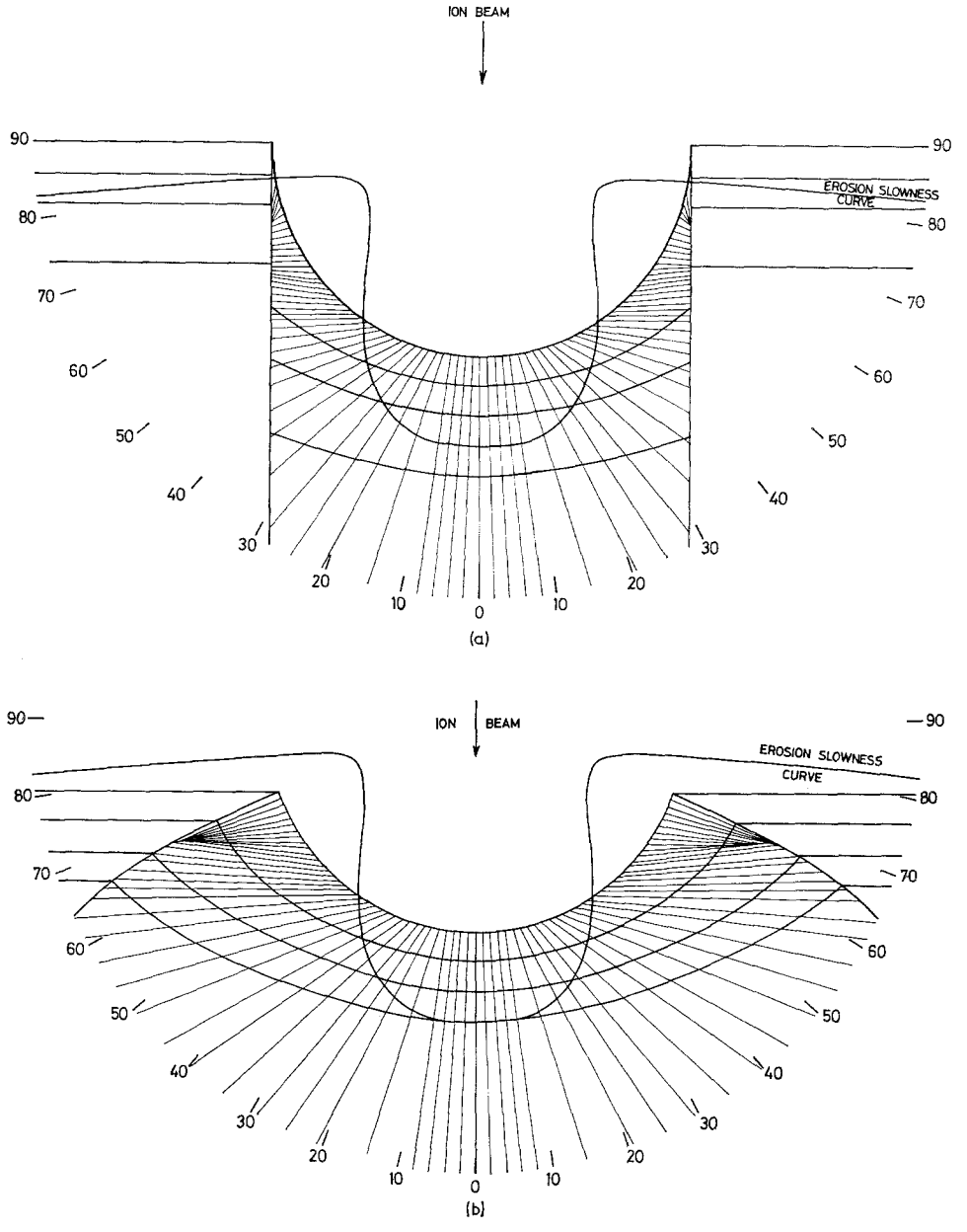

Figure 3 Erosion slowness curve, trajectories and evolved profiles of (a) a full and (b) a partial hemispherical trough on a silica glass surface due to sputtering.

surface indicates a polishing process, with the peaky topography progressing towards flatness. This we feel is the more accurate description of what actually goes on during the bombardment of a sinusoidal surface than that reported by Catana *et al.* [13] whose computer simulation predicts an equilibrium topography of a sharp peak and a plateau. The difference is certainly not a consequence of the exact form of sputtering curve but rather a spurious result arising in the computational procedure.

3.2. Rotation of specimen

We shall apply Frank's kinematic theorems to the hummocky appearance of a rotating silica glass surface undergoing bombardment at

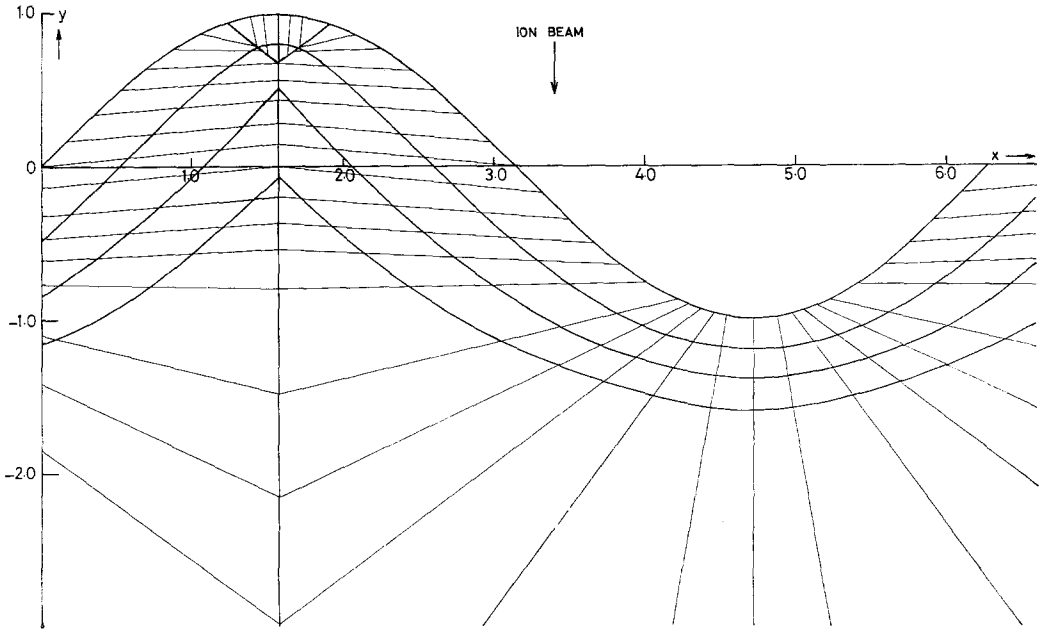

Figure 4 The evolution of sputtered shapes from an initial sinusoidal glass surface during ion bombardment. The "dissolution" trajectories are also shown.

approximately 60° to the surface normal as reported earlier [8]. Fig. 5 shows a hummock on a flat surface rotating in its plane bombarded by an ion beam of uniform intensity. Let δ be the angle between the surface normal and the rotation axis and θ the angle between the ion beam and the rotation axis. We need to generate the averaged erosion slowness surface. So long as the element of the surface under consideration is convex then we may easily perform the averaging process under the restriction of self-shadowing. Each element of the surface may be described by the angular co-ordinates (δ, ϕ) where ϕ is the azimuthal angle. For a particular θ we need to find the mean value of the sputtering rate as a function of δ by averaging over Φ. If $(\delta + \theta) > \pi/2$ then self shadowing occurs for some part of the rotation cycle and if $(\delta - \theta) > \pi/2$ the surface is permanently shadowed. The resulting averaged slowness surface for $\theta = 60°$ is illustrated in Fig. 6 with the initial hummock shape and resultant topographies superimposed on it. It can be seen that the hummock grows in diameter but the height stays the same as the erosion rate is the same on top of the hummock and on the surrounding plain.

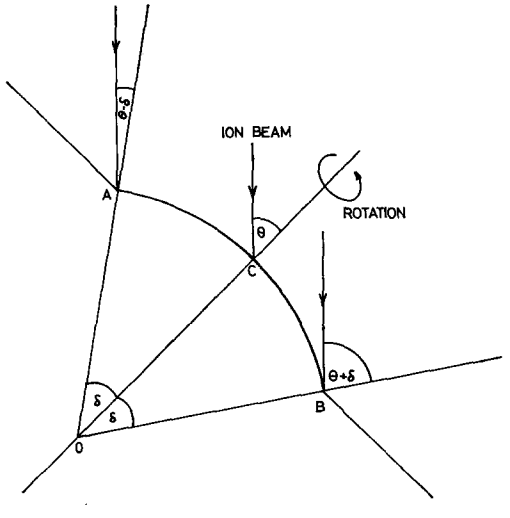

Figure 5 Incidence of ion beam on a surface hummock rotating in its plane about an axis through its centre.

In an earlier paper [8] it was suggested that the apparent growth in height might be due to reflection of the ions from the hummock on to the plain. However, from the scanning micrographs no appreciable annular trough surrounding the periphery of the hummock could be detected. Another possibility is that some sort of sputter protection takes place at the top of the hummock. Again there was no direct evidence for sputter protection, but by examining the possible effects of contaminants adhering to the target

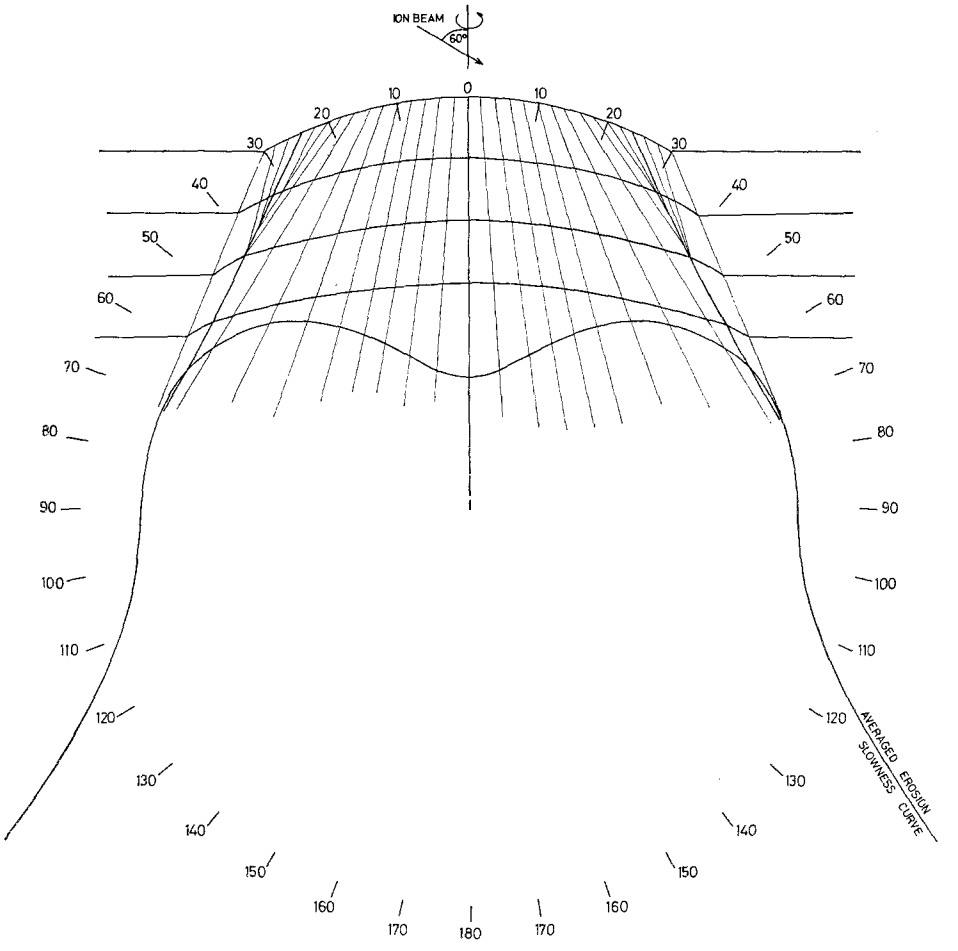

Figure 6 The averaged erosion slowness curve for the case when the ion beam is at 60° with the rotation axis and the evolution of sputtered profiles of a hummock on a glass surface.

surface, its occurrence could be inferred. Fig. 7 shows the effect of chemical etching of a crystal surface with adhering contaminants [20]. The situation (a) corresponds to near-normal incidence, i.e. $\theta \simeq 0$, and to grazing incidence, i.e. $\theta \geqslant 75°$, where the erosion rate decreases rapidly with increase of incidence angle. At normal incidence, no under-cutting will occur as depicted. Similar profiles will result only if the contaminant disintegrates under bombardment. Situation (b) corresponds to sputtering at or near the incidence angle where the erosion is greatest, i.e. $\theta \simeq 70°$. Construction of sputtering trajectories for cases shown in Fig. 7 is beyond the scope of this paper since the erosion rate depends on both position and orientation owing to the shadowing effect by the contaminant. Nevertheless, Fig. 7 leads to the conclusion that hillocks

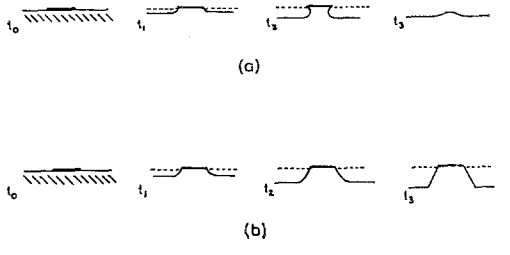

Figure 7 (a) Instability of a hillock due to adhering contamination on a slow-etching crystal surface. (b) Stability of a hillock on a fast-etching crystal surface. Taken from Ives [20].

or hummocks formed at normal incidence or extreme grazing incidence are only transient and will eventually disappear while such irregularities are more persistent at angles of incidence

where sputtering is near maximum. Permanent hillocks will persist at normal incidence only if they obey the conditions depicted in Fig. 8 where the eroded depths of the flat and inclined surfaces are given by the equation

$$d_1 \cos\theta = d_2 . \tag{2}$$

From Equation 1, this means

$$S(0) = S(\theta) . \tag{3}$$

Hence permanent hillocks will form if the half-angle of the apex, α, is equal to $\pi/2 - \theta$, where θ is the angle at which the sputtering yield (atoms/ion) is again equal to that at normal incidence. This is the same conclusion reached by Catana *et al* [13] in their analysis of the computer-simulated topographies.

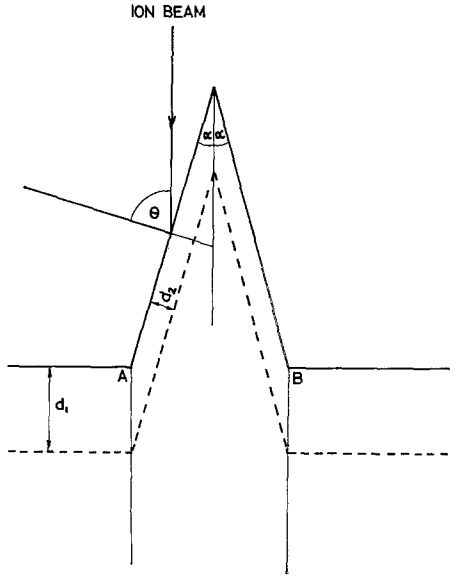

Figure 8 Equilibrium topography of a hillock (or cone) where the trajectories of the intersections A and B are normal to the flat surface.

4. Application to semiconductors: pseudo-isotropic case

We have observed that after prolonged ion erosion initially flat discs of a III-V semiconductor (InP) develop rather complicated topographies. By extending the results of the previous section we are able to give a qualitative explanation of this behaviour. The experimental situation is depicted in Fig. 9. Even in the case of uniform ion beams, uneven attack will occur as a result of the shadows cast by the mask edges. The specimens are therefore dished at the centre by ions coming from all azimuthal directions while the extreme periphery of the dish is only subject to unidirectional attack. In order to take proper account of the erosion process it would again be necessary to investigate the case where erosion is a function of position as well as orientation. However, it is possible to avoid this extension of the analysis by assuming an appropriate general form for the section through a disc after considerable erosion (Fig. 9).

Broadly speaking, we can divide the dished region into three areas centred on the axis of rotation. The specimens were bombarded with

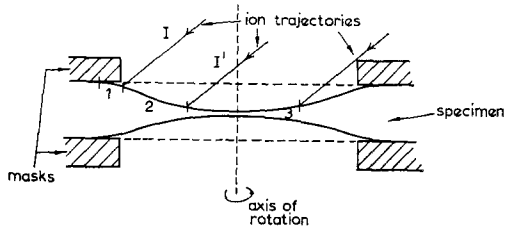

Figure 9 Experimental arrangement for ion bombardment of a flat specimen. The broken lines indicate a section through the specimen at the onset of erosion while the solid lines represent a section through the specimen after an extended period of bombardment. Undercutting of the mask has been deliberately exaggerated.

Ar^+ ions in the energy range 4 to 10 keV and it is well known that this is sufficient to cause severe damage of the surface layers [21]. Observations by transmission electron microscopy revealed that the initially single crystal specimens were turned into fine grained ($\sim$ 200 Å) polycrystals in the damaged region. We are therefore justified in assuming an isotropic slowness surface. In the central region 3, the situation is similar to that depicted in Fig. 5 (the ion beam was incident at $\theta \simeq 60°$) and so flat topped hummocks are produced (Fig. 10a). At the other extreme in region 1 sharply peaked cones are found (Fig. 10b). These have often been observed in the past and are almost certainly caused by surface impurities. Once the eroded area is subject to the variation of azimuthal angle the impurities are undercut (Fig. 7a) and the cones disappear. It remains to discuss region 2. On account of the slope, rotational symmetry is lost and in fact we argue that the most important bombardment will occur for the ion trajectories shown in Fig. 9 between *I* and *I'*. When the specimen is rotated through 180° from the depicted situation either self shadowing

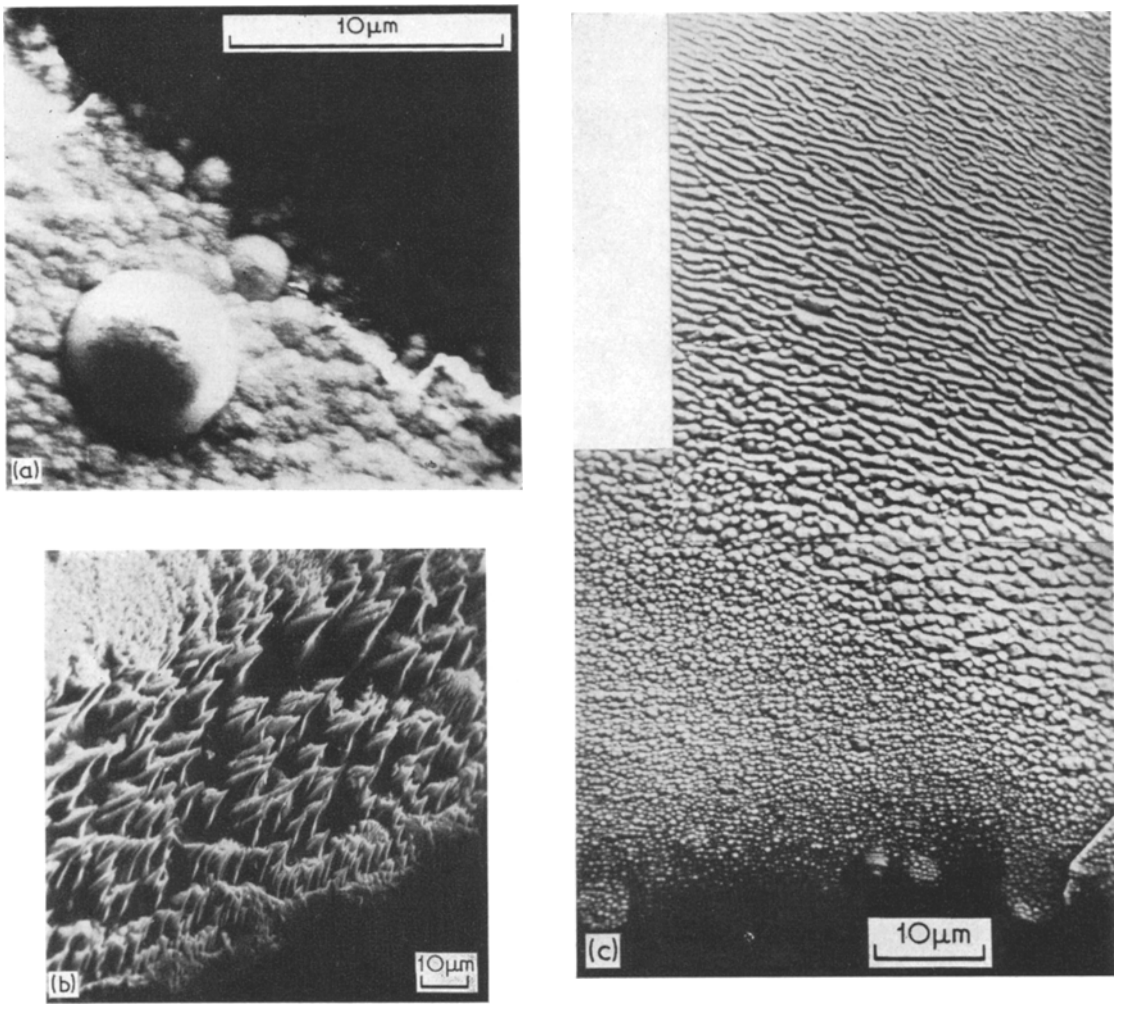

Figure 10 (a) Flat top hummocks formed at the centre of a dish in InP by ion bombardment. (b) Cones produced by unidirectional ion attack near the periphery of the dished region. (c) Hummocks giving way to ridges or steps as the distance away from the axis of rotation increases.

or shadowing by the mask will make erosion relatively unimportant. A typical slope in region 2 is at $\sim 10^\circ$ to the mean surface and hence we perform a slowness surface construction with an angle of 50° between the beam trajectory and the local surface normal. Assuming a sinusoidal starting surface with amplitude chosen to avoid shadowing effects we see that a stepped topography results (Fig. 11, cf. Fig. 10c).

It is well known that a non-crystalline target surface under unidirectional bombardment will develop numerous ridges (similar to stepped topography) perpendicular to the beam at low angles of incidence, and these become parallel to the beam when the incidence angle is altered to grazing. The latter is difficult to explain by the present treatment because in grazing incidence, shadowing effects give rise to an erosion rate which depends on position as well as orientation. Moreover, in order to explain ridges parallel to the beam a three-dimensional analysis is required.

5. Application to metal single crystals: anisotropic case

Although several theories have been advanced for the formation of faceted structures during ion bombardment of metals and alloys, none is really satisfactory. Clearly, focused collision sequences along rows of nearest or next nearest neighbours are the essential physical process

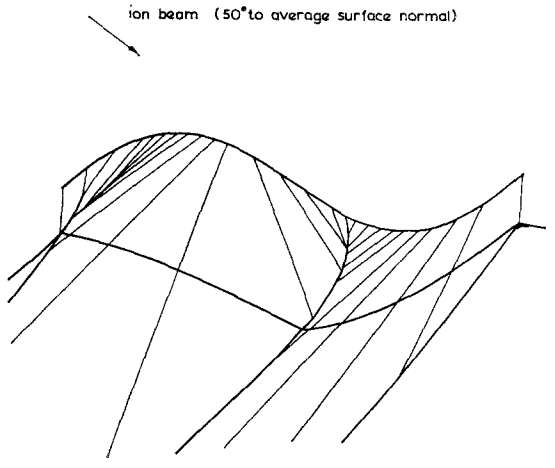

Figure 11 Slowness surface construction showing how a sinusoidal surface erodes to give steps.

involved [22]. One case where difficulties arise is in trying to explain the formation of pyramids on (1 1 1) surfaces of fcc metals when they are bombarded at moderate ion energies ($\gtrsim$ 1 keV). An example is shown in Fig. 12. The experimental situation is well documented: at low energies of bombardment, the pyramids have only three faces which are approximately (1 1 0) planes [23] and the patterns of atomic ejection [24] show three dark spots corresponding to the three $\langle 1\,1\,0 \rangle$ directions at approximately 55° to the surface. As the energy increases, a further symmetrical set of three spots appears in the ejection pattern [25] and at the same time pyramids with six faces may begin to appear on the target surface. Although this second set of sputtering spots is more diffuse than the first, they correspond to much the same angle of atomic ejection from the surface. These observations cover the case of normal incidence [26] as well as other angles of incidence with specimen rotation about the surface normal.

How are the second set of sputtering peaks to be explained? According to one theory [25] twinning occurs in the surface layers as a result of ion damage at the higher energies. However, the configuration of twins necessary to account for the six-faced pyramid in Fig. 12 makes this argument implausible. A second theory [27] uses the idea of bent collision sequences at a (1 1 1) surface. As the energy of bombardment increases [1 0 0] channelling is known to occur and it is to be expected that focused collision sequences will take place along this (the next nearest neighbour) direction. [1 0 0] collision sequences are bent towards [1 1 1] by something like 15° while [1 1 0] collision sequences are bent away by only a small amount and it is argued that one can therefore account for the observed ejection patterns. Unfortunately, this argument fails once the irregular topography is established and then collision sequences emerge almost orthogonal to the relevant surface face. However, if the idea of focused collision sequences is allowed to influence a reconstruction of the slowness surface, a plausible explanation emerges.

We need to decide which surface plane will give rise to the highest rate of atomic ejection. Consider focused collisions occurring along a row making an angle α with the surface. Lattice expansion at the free surface will in general result in bending of the atomic planes, causing deflection of the collision sequence and a reduction in the number of atoms ejected. Consequently the highest sputtering rate occurs when the direction in which the lattice is expanding coincides with the direction of the row, i.e. when $\alpha = 90°$. This is the vital factor overlooked in the isotropic treatment.

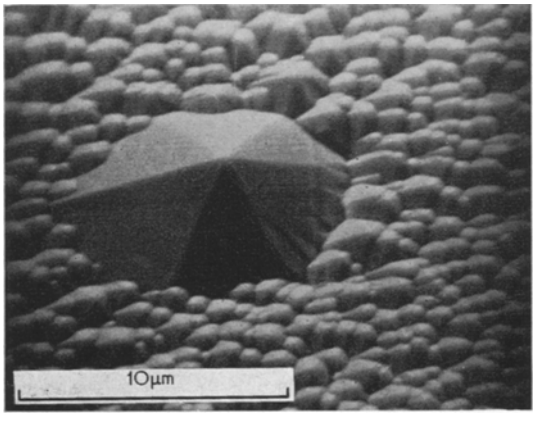

Figure 12 Faceted structure formed on a (1 1 1) face of a AgZn alloy during ion bombardment. Alternate faces are believed to be {1 1 0} planes.

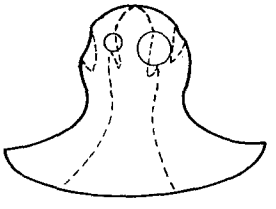

Figure 13 Diagram of expected form of anisotropic slowness surface. Note the existence of saddle points.

An averaged slowness surface is required in the case of a rotated crystal when the beam is directed at an angle to the mean orientation of the (1 1 1) surface. Let us first recall the averaging process in the isotropic case (Section 3.2). For the anisotropic case we need to average over an anisotropic slowness surface $S(\psi,\alpha)$ where ψ is the angle between the normal to the surface element and the incoming ion beam. A sketch of this slowness surface is given in Fig. 13. However, since the shapes of neither the $\langle 1\,1\,0\rangle$ nor the $\langle 0\,0\,1\rangle$ depressions are known, it will suffice for the present to add depressions to the averaged isotropic slowness surface. We consider a $(\bar{1}\,1\,0)$ section through the averaged surface, and add a relatively sharp depression

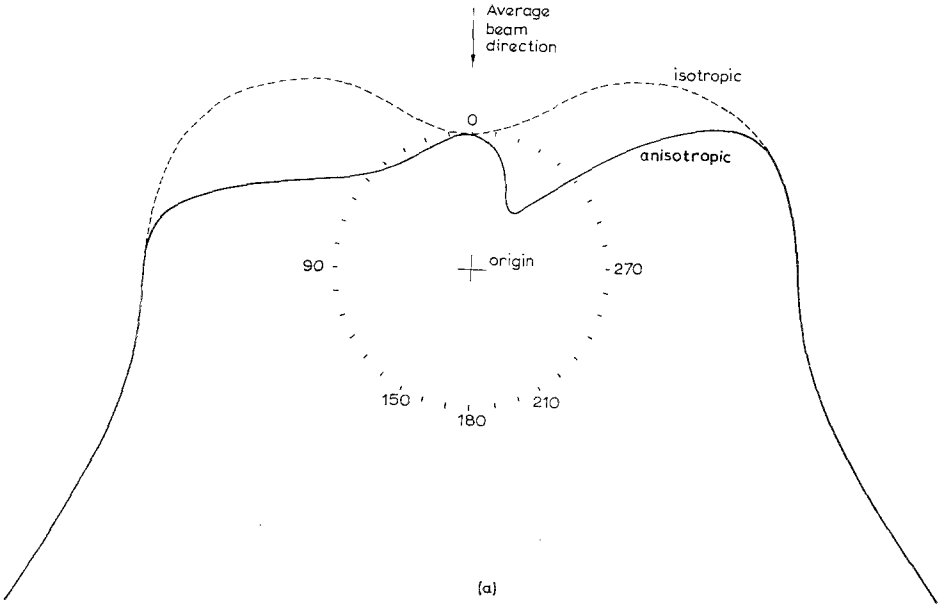

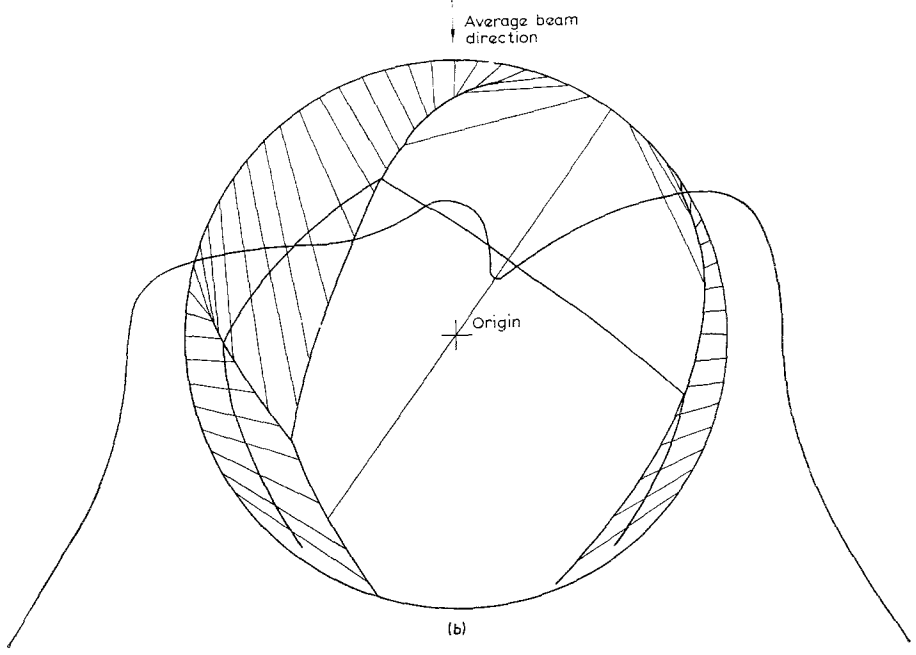

Figure 14 (a) {1 1 0} section through a rotation averaged slowness surface with added depressions due to focusons. (b) Erosion of a cylinder using the anisotropic slowness surface in (a).

with a minimum along [110] and a much broader depression with greatest reduction along [001]. These depressions on the slowness surface correspond to positions where focusing directions meet the actual surface at right angles. Finally, we make constructions on the resulting slowness surface to discover how a sphere would be eroded.

In Fig. 14 we illustrate the effect of ion erosion of a cylinder. Facets appear at approximately the required angles to (111). However, in the case of a sphere the (110) facets out of the plane of Fig. 14 would cut off the (001) facet and give rise to a three-faced pyramid. It therefore seems impossible to account for the six-faced pyramids without allowing for the impurities which must sit at the apex in order to explain why the pyramid stands so much higher than its surroundings.

6. Conclusions

Frank's kinematic theorems provide a simple and yet powerful way of predicting ion-bombarded surface topographies. The principal source of error in this analysis must be in the determination of the slope of the erosion slowness curve from which the trajectories are derived. Moreover, other sputtering mechanisms such as ion reflection and redeposition of sputtered material have not been taken into account. Despite these shortcomings, the predicted topographies show remarkably good agreement with experimental observations.

Acknowledgements

We would like to thank the National Physical Laboratory for financial support (I.S.T.T.) and Dr P. J. Tufton of the Royal Radar Establishment, Malvern, for the provision of indium phosphide specimens.

References

1. D. J. BARBER, *J. Mater. Sci.* **5** (1970) 1.
2. M. PAULUS and F. REVERCHON, "Le Bombardement Ionique" (C.N.R.S., France, 1962) p. 223.
3. J. B. SCHROEDER, H. D. DIESELMAN, and J. W. DOUGLASS, *Appl. Optics* **10** (1971) 295.
4. A. R. BAYLY and P. D. TOWNSEND, *Opt. and Laser Technol.* **2** (1970) 117.
5. A. D. G. STEWART and M. W. THOMPSON, *J. Mater. Sci.* **4** (1969) 56.
6. I. H. WILSON and M. W. KIDD, *ibid* **6** (1971) 1362.
7. A. R. BAYLY, *ibid* **7** (1972) 404.
8. I. S. T. TSONG and D. J. BARBER, *ibid* **7** (1972) 687.
9. P. J. GOODHEW, *ibid* **8** (1973) 581.
10. G. K. WEHNER and D. J. HAJICEK, *J. Appl Phys.* **42** (1971) 1145.
11. W. HAUFFE, *Phys. Stat. Sol. (a)* **4** (1971) 111.
12. N. HERMANNE and A. ART, *Radiation Effects* **5** (1970) 203.
13. C. CATANA, J. S. COLLIGON, and G. CARTER, *J. Mater. Sci.* **7** (1972) 467.
14. F. C. FRANK, "Growth and Perfection of Crystals" (John Wiley and Sons, New York, 1958) p. 411.
15. *Idem, Z. Phys. Chem. Neue Folge* **77** (1972) 84.
16. F. C. FRANK and M. B. IVES, *J. Appl. Phys.* **31** (1960) 1996.
17. M. B. IVES, *ibid* **32** (1961) 1534.
18. H. BACH, *J. Non-Crystalline Solids* **3** (1970) 1.
19. G. K. WEHNER, *J. Appl. Phys.* **30** (1959) 1762.
20. M. B. IVES, Ph.D. thesis, University of Bristol (1959).
21. G. W. ARNOLD and R. E. WHAN, *Radiation Effects* **7** (1971) 109.
22. R. S. NELSON and M. W. THOMPSON, *Proc. Roy. Soc.* **A259** (1961) 458.
23. G. K. WEHNER, *Phys. Rev.* **102** (1956) 690.
24. G. S. ANDERSON and G. K. WEHNER, *J. Appl. Phys.* **31** (1960) 2305.
25. G. S. ANDERSON, *ibid* **33** (1962) 2017.
26. P. HAYMAN and C. WALDENBURGER, *Compt. Rend. Acad. Sci.* **254** (1962) 486.
27. R. L. CUNNINGHAM and J. NG-YELIM, *J. Appl. Phys.* **40** (1969) 2904.

Received 30 November 1972 and accepted 16 January 1973.